# 4×2 hot electron bolometer mixer arrays for detection at 1.4, 1.9, and 4.7 THz for a balloon borne terahertz observatory

Silva, J.R.G.; Laauwen, W.M.; Mirzaei, B.; Vercruyssen, N.; Finkel, M.; Westerveld, M.; More, N.; Silva, V.; Gao, J.R.; More Authors

**DOI**
10.1117/12.3019197

**Publication date**
2024

**Document Version**
Final published version

**Published in**
Millimeter, Submillimeter, and Far-Infrared Detectors and Instrumentation for Astronomy XII

# 4×2 Hot electron bolometer mixer arrays for detection at 1.4, 1.9 and 4.7 THz for a balloon borne terahertz observatory

J. R.G. Silva[a,c*], W. M. Laauwen[a], B. Mirzaei[a,b], N. Vercruyssen[a,b], M. Finkel[a], M. Westerveld[a], N. More[a], V. Silva[a], A. Young[d], C. Kulesa[d], C. Walker[d], F. van der Tak[a,c], and J. R. Gao[a,b]*

[a]SRON Netherlands Institute for Space Research, Landleven 12, 9747 AD Groningen and Niels Bohrweg 4, 2333 CA Leiden, the Netherlands; [b]Optics Research Group, Department of Imaging Physics, Delft University of Technology, Delft, 2628 CJ, the Netherlands; [c]Kapteyn Astronomical Institute, University of Groningen, Groningen, 9747 AD, the Netherlands; [d]Steward Observatory, University of Arizona, 933 N Cherry Ave, Tucson, AZ 85719, USA

*Contact: j.r.g.d.silva@sron.nl, and j.r.gao@sron.nl

## ABSTRACT

We have demonstrated three 4×2 hot electron bolometer (HEB) mixer arrays for operation at local oscillator (LO) frequencies of 1.4, 1.9 and 4.7 THz, respectively. These arrays consist of spiral antenna coupled NbN HEB mixers combined with elliptical lenses. These are to date the highest pixel count arrays using a quasi-optical coupling scheme at supra-THz frequencies. At 1.4 THz, we obtained an average double sideband mixer noise temperature of 330 K, a mixer conversion loss of 5.2 dB, and an optimum LO power of 210 nW. The array at 1.9 THz has an average mixer noise temperature of 425K, a mixer conversion loss of 6.4 dB, and an optimum LO power of 190 nW. For the array at 4.7 THz we obtained an average mixer noise temperature of 715 K, a mixer conversion loss of 8.9 dB, and an optimum LO power of 240 nW. We found the arrays to be uniform regarding the mixer noise temperature with a standard deviation of 3-4%, the conversion loss with a standard deviation of 8-11%, and optimum LO power with a standard deviation of 5-6%. The noise bandwidth was also measured, being 3.5 GHz for the three arrays. These performances are comparable to previously reported values in the literature for single pixels and also other detector arrays at similar frequencies. Our arrays met the requirements and were employed in the Galactic/Extra-Galactic ULDB Spectroscopic Terahertz Observatory (GUSTO), a NASA balloon borne observatory. GUSTO launched from Antarctica on the 31st December 2023 having a successful flight of 57 days, the longest ever recorded by NASA for such mission profile.

**Keywords:** GUSTO, HEB, lens-antenna, mixer array

## 1. INTRODUCTION

The supra-terahertz (THz) frequency range between 1 and 6 THz is very interesting and important for astronomy because it is rich in diagnostic atomic fine structure lines (e.g., [CII], [NII], [OI]), high-J lines of heavy molecules (e.g., CO) and ground-state lines of hydrides (e.g., H2O, HD) [1]. With the use of high resolution spectroscopic techniques based on a heterodyne receiver, it is possible to measure not only the line intensity but also resolve the frequency line profile that allows to extract information regarding the velocities of interstellar gas clouds. With such detailed information one can unveil the dynamics and processes that dominate, for example, in regions of star and planet formation [2-5]. Another application of heterodyne receivers at terahertz frequencies is interferometry, enabling to spatially resolve objects with a high angular resolution of sub arcsec [6].

The core of a heterodyne receiver is a mixing element, where the sky signal is mixed with a strong and well-known signal from a local oscillator (LO). During the mixing, the sky signal is down converted to the frequency difference between the sky and LO signals, named intermediate frequency (IF). This IF signal is in the GHz range, which makes it easier to be amplified and processed by common electronics. Furthermore, a sufficiently large IF bandwidth is needed for the detection of at least an entire spectral line without the need to tune the LO frequency. At THz frequencies the best performing mixer devices are the superconductor-isolator-superconductor (SIS) junctions [7-8] and the hot electron bolometers (HEBs) [9-10]. SIS mixers are based on photon-assisted tunnelling in the junction, having the highest sensitivity and largest IF

Millimeter, Submillimeter, and Far-Infrared Detectors and Instrumentation for Astronomy XII,
edited by Jonas Zmuidzinas, Jian-Rong Gao, Proc. of SPIE Vol. 13102,
131020I · © 2024 SPIE · 0277-786X · doi: 10.1117/12.3019197

bandwidth among the two types of mixers [11]. Because of this, up to 1 THz SIS mixers are the detector of choice for heterodyne instruments, such as those for Atacama Large Millimeter/submillimeter Array (ALMA) [12]. However, above 1 THz, the performance of such a mixer degrades rapidly due to the finite energy gap of the superconductor used, combined with the increase with frequency of the parasitic reactance of the junction. HEBs are based on the bolometric effect, where a change in the temperature induces a change in the resistance. They do not suffer from the upper frequency limitation, in contrast to SIS, which makes them the mixer of choice for the heterodyne instruments that operate above 1 THz. The best performing HEBs are so far based on the superconducting niobium nitride (NbN) [10], and have been demonstrated up to 5.3 THz [13]. NbN HEBs on Si substrates, with reasonable receiver noise temperatures have shown a typical IF bandwidth of 3-4 GHz [14-15]. Such devices have been previously used in instruments such as HIFI on the Herschel Space Observatory [15-16], the STO-2 balloon borne observatory [17] and upGREAT on the SOFIA air borne observatory [18]. As local oscillators, different coherent source types have been employed depending on the target frequency. For frequencies below ~2 THz the preferred LOs are solid-state sources based on frequency multiplier-chains [19-20] because they can be operated at room temperature and have a sufficiently wide frequency tuning range of $\geq 15\%$ [20]. Starting from ~2 THz, quantum cascade lasers (QCLs) [21-22] dominate because they can be operated at any frequency within the range between 1.3 to 5 THz with sufficient output power. The frequency for the QCLs that were used or are suitable as LO can be tuned electrically by varying the bias voltage. However, the tuning range is so far limited to $\leq 10$ GHz [23], which is only a small fraction of the operating frequency. With novel approaches, e.g., a QCL by applying a metasurface in combination with vertical-external cavity surface-emitting-laser structure, a 20% fractional tuning is possible [24]. Furthermore, THz QCLs are typically operated at temperatures between 40-70 K, which can be provided by Stirling coolers.

With recent advancements in mixer technology, the sensitivity of NbN HEBs has significantly been improved, approaching levels that are only a few times the quantum limit (hf/2k) defined for the single sideband. For instance, at 1.6 THz, our group has demonstrated a considerable improvement in DSB mixer noise temperature, achieving a reduction of approximately 30% relative to previous reports [25], with values as low as 6.2 times hf/2k. Additionally, another study [13] has reported achieving DSB mixer noise temperatures as low as 4.2 times hf/2k at 5.3 THz. Further improvements to a DSB receiver noise temperature, if possible, have a limited room with maximally a factor of ~2 at the high end of the supra-THz frequency range, as suggested in [13]. On the other hand, some of the sources or structures of astronomical interest, e.g., giant molecular clouds, are extended over angular scales much larger than the field of view of a telescope, which need to be scanned or mapped. A single pixel receiver placed at the focal point of the telescope is relatively inefficient as it samples only a small part of the field of view of the telescope. In this case, a multi pixel detector array positioned at the focal plane of a telescope can therefore increase the efficiency of the observatory [26], where the mapping speed of the instrument scales roughly with the number of pixels in the array [27-28]. However, only recent advances in some critical technologies have made receiver systems using multi-pixel arrays possible for airborne [18], balloon borne [29-31], and proposed instruments concepts for future space THz observatories [32-34]. The critical technologies include frequency multiplier-chain based multi-beam LOs [35], high power QCLs [23,36], and LO multiplexing schemes based on Fourier phase gratings [37-38].

Until recently only STO-2 [17] and upGREAT [18] instruments have made use of detector arrays at supra-THz frequencies. STO-2 employed 2-pixel arrays at 1.4 and 1.9 THz, consisting of quasi-optically coupled HEB mixers, namely using a lens-antenna scheme. upGREAT used to operate a 14-pixel array at 1.9 THz, which consisted in practice of two 7-pixel arrays for detecting two orthogonal polarizations. Besides, upGREAT used also a 7-pixel array at 4.7 THz. The upGREAT mixer arrays were based on feedhorn-waveguide structures to couple the radiation from free space to the HEB and were comprised of multiple individual mixers on physically separated blocks. In other words, they are not built on a monolithic block. Such mixers have the advantage of being easier to align and match with the instrument optics, however, they occupy a relatively large volume in the instrument, which is in contrast to the need of space instruments, where small and compact arrays are preferred. Furthermore, with this approach it is hard to realize a much larger array e.g., 64 pixels. Recent work shows potential for monolithic waveguide blocks [38], but no such mixer array has been demonstrated yet.

GUSTO [29-30] was a NASA balloon borne THz observatory that aimed at exploring the inner dynamics of the Milky Way and the Large Magellanic Cloud using three heterodyne array receivers to map the fine structure lines of [NII] at 1.46 THz, referred to as Band 1 (B1), [CII] at 1.9 THz (B2) and [OI] at 4.7 THz (B3). GUSTO launched from the Long Duration Ballon facility in Antarctica on the 31st December 2023 with a successful flight of 57 days, the longest ever recorded for this type of missions. GUSTO used compact 4x2 HEB mixer arrays. As LOs, for B1 and B2, it used frequency multiplier chain arrays developed by Virginia Diodes Inc, Charlottesville in USA [35]. For the B3 receiver, it employed a multi beam

LO in a 4x2 pattern generated using a QCL developed by MIT at Cambridge in USA [23], which was multiplexed by an asymmetric Fourier phase grating developed by SRON/TUDelft [38].

The focus of this paper is the lab characterization of the three 4x2 HEB mixer arrays (with 24 pixels in total) developed for the GUSTO receivers. Due to technical issues and mission deadline not all pixels were used during the final flight. Therefore, we believe it is the best that the array performance during GUSTO's integration and flight will be described in a separate paper.

We focus our characterization on the DSB mixer noise temperature ($T_{mixer}^{DSB}$), the mixer conversion loss ($L_{mixer}^{DSB}$) and the optimum LO power requirement ($P_{LO}$) at the mixer array level. These parameters represent the figures of merit used in the requirements set for the HEB mixers needed for GUSTO. The goal in the development of these array was to meet the instrument performance requirements. These arrays use a quasi-optical coupling scheme based on an elliptical lens combined with a logarithmic spiral antenna, making them the largest quasi-optical mixer arrays in the supra-THz region so far. The architecture used in our arrays also enables to seamlessly scale into high pixel count (>64 pixels) as will be discussed at the end of the paper.

Our paper is organized as follows. In Section II we start by introducing the instrument requirements, the different array architectures and then describe the assembled detector arrays. In Section III we highlight the experimental setup used to characterize the arrays. Section IV presents the characterization results of the arrays. The paper ends with the conclusions.

## 2. HEB MIXER ARRAYS

In Table 1 we summarize the performance requirements of the HEB mixer arrays for GUSTO regarding sensitivity, LO power and IF bandwidth. GUSTO scientific goals required an average single sideband (SSB) system noise temperature ($T_{sys}^{SSB}$) of 2900 K at 1.46, 2700 K at 1.9 THz, and 3000 K at 4.7 THz. These requirements can be broken down into allocations at the mixer array level in the form of a pair, $T_{mixer}^{DSB}$ and $L_{mixer}^{DSB}$, for each array, shown in Table 1. Here we define $T_{mixer}^{DSB}$ as the noise temperature after removing the contribution caused by the optical losses in front of the lens and the noise contribution from the IF chain. This value is defined at an IF frequency of 2 GHz. We focus on quantifying and discussing both $T_{mixer}^{DSB}$ and $L_{mixer}^{DSB}$ because they are intrinsic to the array, being independent of the optics used in a test setup. These are figures that allow for a much easier comparison of performance of the same mixers between different systems.

Table 1. GUSTO RF and IF requirements for each pixel in the HEB mixer arrays. $T_{mixer}^{DSB}$ and $L_{mixer}^{DSB}$ are the pixel noise temperature and conversion loss, respectively, defined in front of the lens, see main text. $T_{mixer}^{DSB}$ is defined at an IF frequency of 2 GHz. $P_{LO}$ is the mixer optimum LO power at the HEB.

| Lens type | Operating Frequency (THz) | $T_{mixer}^{DSB}$ (K) | $L_{mixer}^{DSB}$ (dB) | $P_{LO}$ (nW) | IF bandwidth (GHz) |
|---|---|---|---|---|---|
| B1 | 1.46 | 650 | 10.5 | 155-270 | 3 |
| B2 | 1.9 | 650 | 10.5 | 155-270 | 3 |
| B3 | 4.7 | 700 | 11 | 155-270 | 4 |

All HEB mixer arrays were designed to allow for eight pixels in a 4×2 configuration within a single metal block. All the pixels in an array share the same basic configuration that is shown in Figure 1a. For each pixel THz radiation is collected on the surface of the elliptical Si lens. It is then focused, as it propagates through the lens and HEB chip substrate, to the spiral antenna, where the radiation is converted to an AC electrical current that is fed to the HEB. Through bonding wires, the HEB is connected to a co-planar waveguide (CPW) line that is used to both DC bias the device and collect the IF signal from the mixer. Each pixel is terminated with an IF connector that acts as the interface to a low noise amplifier (LNA). In the array the IF lines are placed such that no IF cross talk is present in the assembled circuit board. To confirm this, we measured a $S_{21}$ < -60dB, where $S_{21}$ represents the power transferred from Port 1 to Port 2, with each port in our case being a different IF line.

The lenses and the substrate of the HEB chips are made of pure, highly resistive Si (≥5 kΩ·cm), which has a negligible optical loss at cryogenic temperatures [40]. Each HEB chip consists of a NbN bridge integrated with a planar logarithmic spiral antenna. We chose such an antenna because it has a high power coupling efficiency to the HEB bridge over a wide range from 1 THz to 5.3 THz [13,41,42]. Other options, such as twin slot antennas, have never been demonstrated for low

noise HEB mixers above 2.5 THz [43]. Additionally, because of the wide-band coverage of a spiral antenna, we can apply a common design for the arrays operated at the three different frequencies, which reduces the cost significantly. The antenna structure is similar to the one used in [41]. Some details of the antenna are given in [44]. Elliptical lenses were chosen since they offer high coupling of the radiation to an antenna and also higher gaussicity of the beam compared to a hemispherical lens [45].

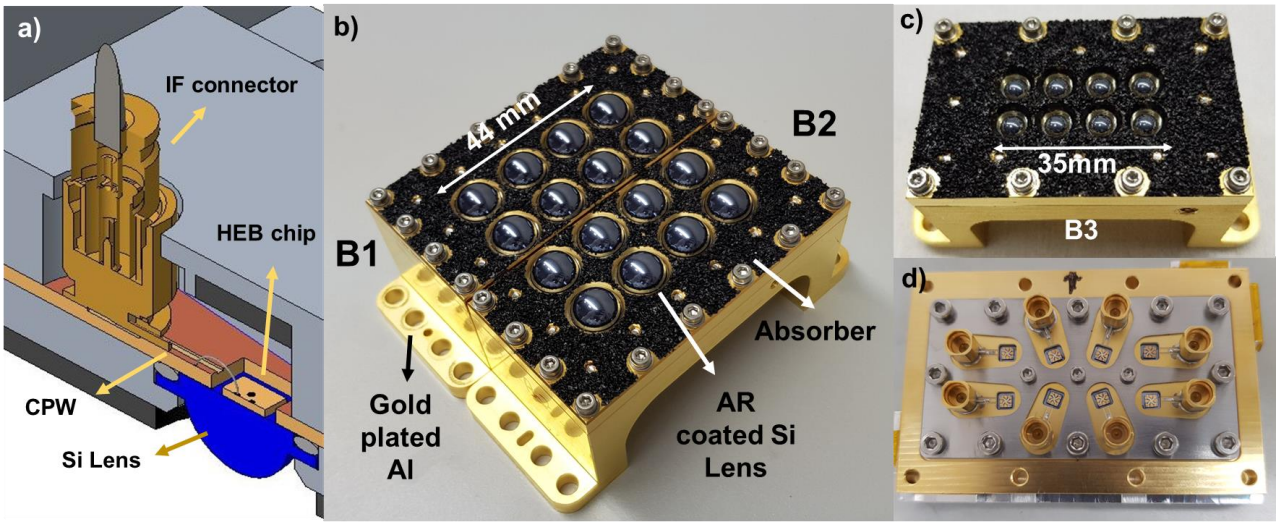


Figure 1. 4×2 HEB mixer arrays. a) Schematic of the single pixel configuration used in all the arrays. THz radiation is collected at the elliptical surface of the lens and focused to the HEB antenna. The HEB is connected through bonding wires to a co-planar waveguide (CPW) transmission line, which is used to both bias the device and carry out the IF signal from the mixer. The other end of the CPW line is terminated with an IF connector that is the interface to a low noise amplifier. b) Completed B1 and B2 arrays, for operation at 1.46 and 1.9 THz, respectively. The arrays are presented side by side, mimicking a 4×4 array. This is the actual placement on the cold plate of the GUSTO instrument. c) Completed B3 array designed to operate at 4.7 THz. d) A back side view of the partly assembled B3 array, where the eight HEB chips, CPW lines and IF connectors are shown, from [48].

Two models of detector arrays were designed to accommodate the two types of lenses with different diameters. In Figure. 1b we show the completed B1 and B2 arrays, using 10 mm diameter lenses and having a pitch size of 11 mm. The two arrays make use of the same model and were optimized for operation at 1.46 and 1.9 THz, respectively. Because these two frequencies are very close, it is difficult to separate them in the optical path of the instrument. Thus, B1 and B2 were designed to be placed side by side on the cold plate of the cryostat, mimicking a 4×4 array. The devices used have a NbN bridge of 2 μm in width, 0.15 μm in length, and 5 nm in thickness. Besides a good impedance matching between the HEBs and the antennas, such dimensions of the HEBs provide an optimum LO power within the requirements described in Table 1. The critical temperature of the NbN bridges is about 10 K. In Figure 1c we show the completed B3 array that uses 5 mm diameter lenses and has an 8 mm pitch size. This array is optimized for operation at 4.7 THz. In Figure 1d we present a back side view of the B3 array, while partly assembled, where the eight detector chips, CPW lines and IF connectors are shown. The HEB devices used in this array are similar to the ones used in the other arrays (from the same wafer), however, the NbN bridge lengths are longer, being 0.2 μm instead. The increased HEB length increases the volume of the HEB, and thus the LO power required.

Each of the arrays has a different lens design, optimized to meet the GUSTO optical beam requirements. The optimization study and verification can be found in [46]. The detailed lens designs are shown in Table 2. Additionally, each lens is coated with Parylene C as an anti-reflection (AR) coating with the ideal thickness, designed using Equation 2 in [47]. Both realized (measured) and designed thicknesses of the Parylene C are also shown in Table 2. The differences are due to the limited accuracy in controlling the thickness during the coating process. The methodology used to mount and align HEB antenna with the lens optical axis has been described elsewhere [48].

Table 2. Characteristic parameters of the lenses and AR coating for three different frequencies. Each lens type is used in a different array. The extension length includes the detector substrate, which has a thickness of 342 ±2 µm. For the Parylene-C we present first the realized thickness and in parentheses the ideal, designed thickness.

| Lens type | Operating Frequency (THz) | Major axis (µm) ±2 µm | Minor axis (µm) ±2 µm | Extension length (µm) ±2 µm | Parylene-C thickness (µm) ±0.2 µm |
|---|---|---|---|---|---|
| B1 | 1.46 | 5235 | 5000 | 1542 | 33 (31.7) |
| B2 | 1.9 | 5235 | 5000 | 1527 | 24.5 (24.4) |
| B3 | 4.7 | 2617 | 2500 | 767 | 2.0 (9.8) |

## 3. EXPERIMENTAL SETUP

We measure the DSB receiver noise temperature ($T_{rec}^{DSB}$), the receiver conversion loss ($L_{rec}^{DSB}$), and the required LO power ($P_{LO}$) for each pixel in the arrays. The measurements for the three arrays were performed at 1.39, 1.63 and 5.25 THz, respectively, being slightly different from GUSTO's respective B1, B2, and B3 center frequencies. Since we do not have the same LOs as GUSTO available at SRON (where the experiments were performed), the choice of characterization frequency for the different mixer arrays was limited to the closest THz lines available from the far infrared (FIR) gas laser used as LO in our heterodyne measurement setup. The IF noise bandwidth (NBW) was measured in the IF frequency range between 0.5 and 5 GHz for a few selected mixers. Additionally, the beam properties and pointing direction of the mixers were also characterized and can be found elsewhere [46,48].

The heterodyne measurement setup used in our experiments is schematically presented in Figure 2. The LO is a FIR gas laser operated at 1.39, 1.63 or 5.25 THz. We use a swing arm optical attenuator [49] in combination with a proportional-integral-derivative feedback loop to sweep or stabilize the LO power when measuring $T_{rec}^{DSB}$ [50]. This methodology allows for sweeping the current of a HEB at a given voltage for both the hot and cold load measurements, thereby determining the Y-factor at the exact same DC bias point without being influenced by fluctuations and drift in the FIR laser power. Using this approach, the same current is achieved by making a small adjustment in LO power to compensate for the power difference coupled to the detector between the hot and cold load. Conceptually, since the LO power is different, the mixer gain also changes. However, measurements with a similar device, where we added an optical narrow bandpass filter, showed that after correcting for the optics, we obtained very similar noise temperatures in both cases. This indicates that our methodology is valid. The reason is that the LO power change is very small, on the order of 2-4%, causing a negligible change in mixer gain. This observation aligns with previous studies from our group [51,52].

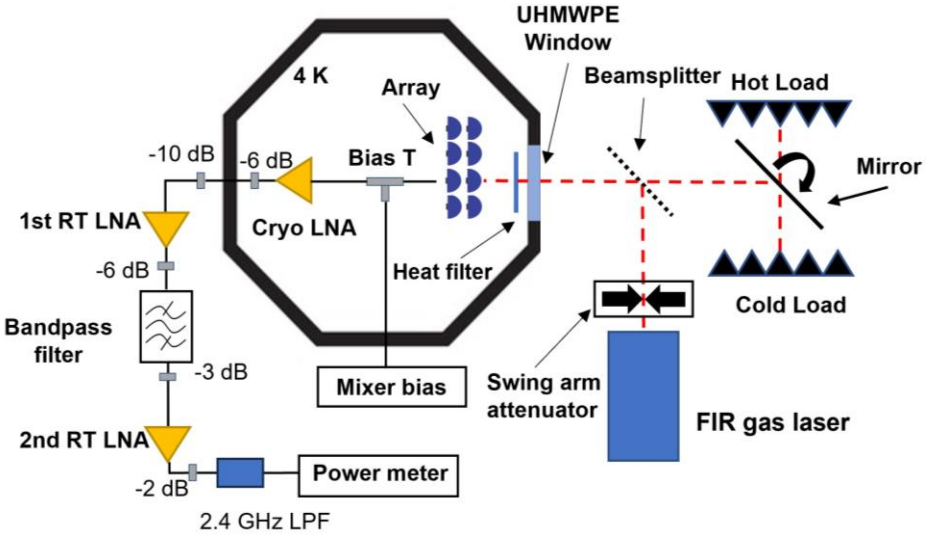


Figure 2. Experimental setup for measuring double sideband receiver noise temperature ($T_{rec}^{DSB}$), receiver conversion loss ($L_{rec}^{DSB}$) and optimum local oscillator power ($P_{LO}$). The hot and cold loads and the beam splitter are in air. We use the rotating mirror to change

between the hot and cold load. The IF noise bandwidth was measured using the same setup, but the part including the Band pass filter, 2nd RT LNA, 2.4 GHz LPF and the power meter is replaced with a spectrum analyzer.

The radiation from both the LO and the blackbody load, being either hot (at a temperature of 290-295 K) or cold (77K), are combined with a 3 µm thick Mylar beam splitter. The combined radiation propagates through a 1.2 mm thick ultra-high molecular-weight polyethylene (UHMWPE) cryostat window and a QMC heat filter with a cut-off frequency of 5.8 THz at 4 K, to the lens of the pixel being measured. The total air distance between the hot or cold load and the window of the cryostat is ≈30 cm. In the schematic we also show an array, which is mounted on the 4K plate of the cryostat. However, only one pixel could be measured at a time since we could not perform the measurements of all the pixels simultaneously, limited by our setup. The physical temperature of the mixers during the measurements was 4.3 K for B3 and 5.2-5.4 K for B1 and B2. The reason for this variation was caused by the need to use an interface plate that in the case of B1 and B2 had a reduced thermal conductance to the cold plate when compared to the one used for B3.

The IF chain consists of a bias-T and a cryogenic SiGe low noise amplifier (LNA) [50]. The latter is connected thermally to the 4 K plate. The room temperature part of the IF chain includes two LNAs, a bandpass filter, a 2.4 GHz low pass filter (LPF) and a microwave power meter. For $T_{rec}^{DSB}$ measurements the IF was filtered by the bandpass filter with a bandwidth of 100 MHz, centered at 2 GHz. The IF chain had a total gain of 85 dB and a noise temperature of 6.5 K at 2 GHz. For the noise bandwidth measurements, we replaced the components from the bandpass filter up to the power meter in Figure 2 with a spectrum analyzer.

## 4. RESULTS AND DISCUSSION

### 4.1. Pixel Characterization and analysis

In Figure 3 we present, as an example, the characterization of an HEB mixer from the B3 array at 5.25 THz. Figure 3a shows three measured current-voltage (IV) curves of the HEB in the unpumped state, when no LO is applied, and two pumping states around the optimum $P_{LO}$, where the $T_{rec}^{DSB}$ becomes the lowest. The $T_{rec}^{DSB}$ is obtained using the Y-factor technique, where for a given bias of voltage and current the receiver output powers of the HEB in response to the hot load ($P_{hot}$) and the cold load ($P_{cold}$) are measured. We then obtain the Y-factor by calculating the ratio between $P_{hot}$ and $P_{cold}$, where the Callen-Welton blackbody temperatures are used [51]. In Figure 3b we present an example of a Y-factor measurement for the same pixel. In this case the lowest $T_{rec}^{DSB}$ is 2110 ± 100 K when the device is biased at a current of 32 µA and a voltage of 1 mV. For this particular bias point the $L_{rec}^{DSB}$, obtained using a modified version [53] of the U factor technique [54] is 12.7 ± 0.4 dB. Applying the modified U factor technique we do not require the use of a circulator. The details on our methodology and validity are described in Appendix I of this paper. Using the isothermal technique [55] we estimate the $P_{LO}$ for the same mixer to be between 192-199 nW. The optimal operation region in the IV, where we obtain less than 5% degradation of the $T_{rec}^{DSB}$, covers a voltage range between 0.6 - 1.0 mV and currents between 28-40 µA, which is highlighted in Figure 3a.

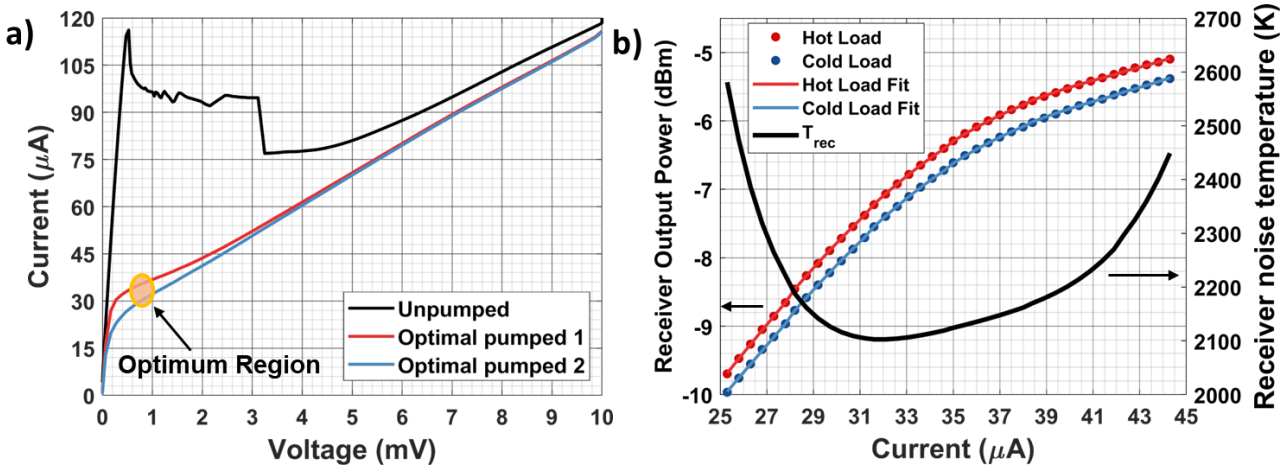


Figure 3. Characterization of a mixer out of the B3 array at 5.3 THz. a) Unpumped and optimally pumped current-voltage curves. Highlighted optimum region, where the $T_{rec}^{DSB}$ degrades less than 5% from the lowest value. b) Measured receiver output powers,

responding to both hot and cold loads, are plotted as a function of current at a bias voltage of 1 mV and respective polynomial fit as a function of the HEB bias current, and the resulting $T_{rec}^{DSB}$.

As discussed in the previous section we are interested in $T_{mixer}^{DSB}$ and $L_{mixer}^{DSB}$. To derive $T_{mixer}^{DSB}$ from the measured $T_{rec}^{DSB}$ and $L_{rec}^{DSB}$, we apply the well-established equation in [1] as follows:

$$T_{mixer}^{DSB} = \frac{T_{rec}^{DSB} - T_{Opt} - T_{IF} \times L_{rec}^{DSB}}{L_{Opt}} \qquad (1)$$

where $T_{Opt}$ and $L_{Opt}$ are the noise temperature and losses, respectively, caused by the optics in the optical path between the hot/cold load and the Si lens as shown in Figure 2, and TIF is the noise temperature from the IF chain (6.5 K). The optical losses at different frequencies in our measurements are summarized in Table 3. By applying Eq. (1), we obtain the $T_{mixer}^{DSB}$, which is essentially the result of subtracting the noise contributions from all the optics in front of the Si lens and the IF chain. For clarity, we stress again that the derived $T_{mixer}^{DSB}$ in this way includes both the optical loss of the Si lens and power coupling loss between the antenna and the bolometer. This is different from the intrinsic mixer noise temperature that is determined by the HEB itself.

Table 3. Optical losses including the air, 3 μm thick Mylar beam splitter (BS), window at room temperature, and the heat filter at 4K in our heterodyne measurement setup. Among them, BS losses are simulated, air loss at 5.3 THz was measured, while the air losses at the other two frequencies are simulated. The remaining loss values are measured.

| Array | LO Frequency (THz) | Air (dB) | Mylar BS (dB) | Window (dB) | Heat Filter (dB) | Total optical losses (dB) |
|---|---|---|---|---|---|---|
| B1 | 1.39 | 0.87 | 0.07 | 0.43 | 0.66 | 2.03 |
| B2 | 1.63 | 0.64 | 0.09 | 0.38 | 1.14 | 2.25 |
| B3 | 5.25 | 0.9 | 0.63 | 1.47 | 0.56 | 3.56 |

Since the B2 and B3 arrays were characterized at different frequencies from the GUSTO frequencies, we need to convert between them in order to compare with the required performance by GUSTO. For the B2 pixels we estimate a 5% higher $T_{mixer}^{DSB}$ at 1.9 THz than what measured at 1.63 THz based on the work in [13]. For the B3 pixels, we estimate a 7.5 % lower $T_{mixer}^{DSB}$ at 4.7 THz than what was obtained at 5.25 THz. The difference was established by measuring the $T_{rec}^{DSB}$ of a similar mixer at both 4.7 THz and 5.25 THz, which is described in [56]. For B1 array, the difference in frequency between the LO used for characterization and LO of B1 is so small that no conversion is required.

To illustrate how we derive a $T_{mixer}^{DSB}$ from a measured $T_{rec}^{DSB}$, we take the same B3 array pixel used for the measurements in Figure 3, as an example. We first apply Eq. (1) to the lowest measured $T_{rec}^{DSB}$(2100K), using Topt = 342K, $L_{rec}^{DSB}$ = 13.6dB and $L_{Opt}^{DSB}$ = 3.56 dB, to derive the $T_{mixer}^{DSB}$ at 5.3 THz. Afterwards by applying a reduction factor of 0.925 (corresponding to 7.5%) to the data at 5.3 THz, we derive a $T_{mixer}^{DSB}$ at 4.7 THz, which is 665 ± 40K.

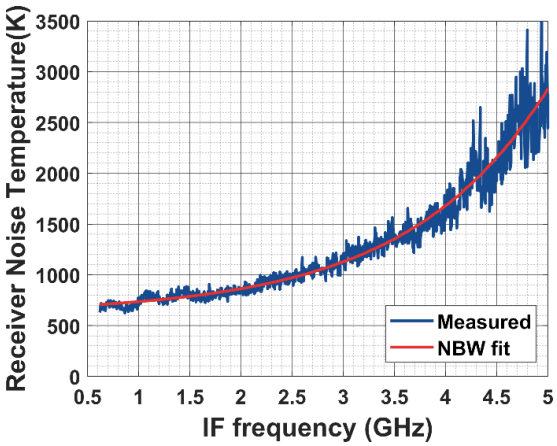


Figure 4. NBW measurement for a B1 pixel at 1.39 THz. The measured receiver noise temperature as a function of the IF frequency was fitted with a generic exponential equation. From the fitted curve, we estimate a NBW of 3.5 GHz, defined as the frequency at which the receiver noise temperature increases by 3 dB.

To measure the NBW of an HEB mixer in our arrays we repeat the $T_{rec}^{DSB}$ measurements over a wide IF range when it is biased at an optimal operating point. In Figure 4 we show one measurement for a B1 pixel at 1.39 THz, where the measured $T_{rec}^{DSB}$ is plotted as a function of IF frequency. By fitting a generic exponential equation, $T_{rec}^{DSB} = T_0 + a * \exp\left(\frac{f}{b}\right)$, to the measured data, we find the frequency where the fitted $T_{rec}^{DSB}$ increases by 3 dB, which determines the NBW and is 3.5 GHz. We obtained the same NBW value for a B3 pixel measured at 5.25 THz, which confirms the data at 1.39 THz. The measured NBW is sufficient to fully meet the IF bandwidth requirements for B1 and B2 arrays for GUSTO but is slightly smaller than what is required for B3. We would like to argue that this NBW is expected because it is limited by the NbN film technology, specifically due to the film thickness of 5-6 nm in practice [57,58] and a Si substrate used. The measured NBW here is close to the one previously reported in an NbN HEB produced in our labs from a different film in [59], which was 4 GHz at 4.7 THz. It also agrees with the NBW results reported for the mixers used in upGREAT, which were 4 GHz for the mixers at 1.9 and 4.7 THz [18], and those in [60], which were between 3 and 3.5 GHz.

### 4.2. HEB Mixer arrays results

The average and standard deviation value for the measured $T_{rec}^{DSB}$, $L_{rec}^{DSB}$ and PLO for all the pixels in the three arrays are summarized in Table 4.

Table 4. Measurement summary of the three HEB mixer arrays averaged over the 8 pixels in an array. It includes the measured received noise temperature ($T_{rec}^{DSB}$) and receiver conversion loss ($L_{rec}^{DSB}$) at 2 GHz IF, and optimum LO power at HEB ($P_{LO}$). In parentheses are the standard deviations within the respective array.

| Array | Measurement Frequency | $T_{rec}^{DSB}$ (K) | $L_{rec}^{DSB}$ (dB) | $P_{LO}$ (nW) |
|---|---|---|---|---|
| B1 | 1.39 THz | 700 (19) | 7.3 (0.6) | 210 (12) |
| B2 | 1.63 THz | 870 (28) | 8.8 (0.7) | 190 (10) |
| B3 | 5.25 THz | 2190 (74) | 12.5 (0.7) | 240 (15) |

We then applied the same methodology described in the previous section to derive the performance for all pixels in the arrays, converting these to the respective operating frequencies in GUSTO. The converted performance data are presented in Figure 5, which shows the performance for all the pixels in the three arrays at the GUSTO operating frequencies. Here, $T_{mixer}^{DSB}$ are shown in (a), $L_{mixer}^{DSB}$ in (b), and $P_{LO}$ in (c). For $P_{LO}$, this parameter remains constant as long as the detector is operated at the same bias point and physical temperature. This means the measured $P_{LO}$ value for each array is constant even if operated at different THz frequencies.

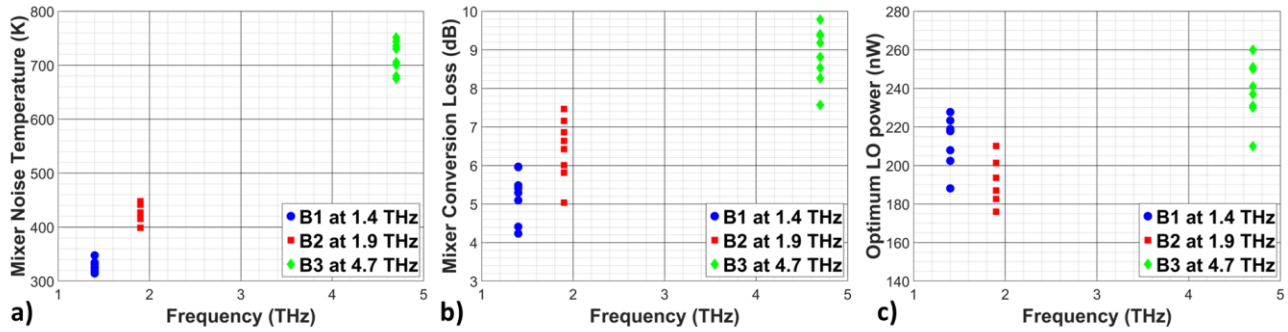


Figure 5. Mixer noise temperature at 2 GHz IF (a), mixer conversion loss (b), and optimum LO power (c) for the different elements of three HEB mixer arrays characterized at GUSTO's frequencies, 1.46, 1.9 and 4.7 THz.

To illustrate the array performance, we summarize the average and standard deviation values of $T_{mixer}^{DSB}$ and $L_{mixer}^{DSB}$ for each array in Table 5, along with the expected performance in the GUSTO receiver.

Table 5. Performance summary of the three HEB mixer arrays averaged over the 8 pixels in an array. It includes the measured mixer noise temperature $\left(T_{mixer}^{DSB}\right)$ and mixer conversion loss $\left(L_{mixer}^{DSB}\right)$ at 2 GHz IF, the receiver noise temperature ( $T_{rec,GUSTO}^{DSB}$) , which was estimated when we apply the GUSTO optics and the measured $T_{mixer}^{DSB}$ and $L_{mixer}^{DSB}$. In parentheses are the standard deviations within the respective array.

| Array | Operating Frequency | $T_{mixer}^{DSB}$ (K) | $L_{mixer}^{DSB}$ (dB) | $T_{rec,GUSTO}^{DSB}$(K) |
|---|---|---|---|---|
| B1 | 1.46 THz | 330 (10) | 5.2 (0.6) | ≈750 |
| B2 | 1.9 THz | 425 (14) | 6.4 (0.7) | ≈1000 |
| B3 | 4.7 THz | 715 (27) | 8.9 (0.7) | ≈1650 |

The average $T_{mixer}^{DSB}$for B1, B2, and B3 arrays are 330 K, 425K, and 715 K, respectively. We demonstrate the arrays uniformity on $T_{mixer}^{DSB}$ in Figure 5a, where their standard deviations are within a range of 3 to 4% for the three arrays. An increase of the $T_{mixer}^{DSB}$ with the operating frequency is expected. However, the value at 4.7 THz is a factor of 2.1 times more than that at 1.46 THz, which is more than was reported in [13], where the factor for the two same frequencies was about 1.7. This suggests that the increase in $T_{mixer}^{DSB}$ is partly due to the contribution of quantum noise and partly due to the additional losses within the mixer, as indicated by the higher $L_{mixer}^{DSB}$ at 4.7 THz. The additional losses at 4.7 THz are expected to be caused by the loss in the antenna and the use of the smaller Si lenses (5 mm) [61]. The former will be discussed in the next paragraphs. In terms of using the unit of quantum noise (hf/2k), they are 9.4x hf/2k at 1.46 THz and 6.2x hf/2k at 4.7 THz.

For $L_{mixer}^{DSB}$, we find that its value increases with the array operating frequency. Such an increase is confirmed even in the intrinsic $L_{mixer}^{DSB}$ after removing the optical loss of the lens and coupling loss between antenna and HEB. This result contradicts the expectation for NbN HEBs since it should be independent of the operating frequency as long as the LO frequency is above the gap frequency of the thin NbN [13,62]. Based on scanning electron microscopy images of some of our devices, we have noticed some artifacts that are present around the gold spiral antenna arms, which may introduce additional ohmic losses to the THz RF current. This effect would be stronger for a higher frequency and thus could introduce additional RF loss, which was not included in our analysis. Furthermore, we notice a relatively large variation on $L_{mixer}^{DSB}$ within an array in Figure 5b, where standard deviations of 8-11% are found for the three arrays. We believe this might be caused by the absence of a circulator in the U-factor measurements, where the circulator is crucial to eliminate standing waves between the HEB and the cryogenic LNA. Without a circulator, the changes in the output impedance of an HEB can change the standing wave behavior, affecting the determination of $L_{mixer}^{DSB}$.

The $P_{LO}$ for the B3 array is slightly higher than that for B1 and B2 due to the greater length of the HEBs used in the B3 array. Within a given array the $P_{LO}$ distribution is uniform, with a standard deviation around 5-6% consistently for the three arrays. However, for B1 and B3 arrays we do have one outlier pixel for each array as shown in Figure 5c. Nevertheless, even with these two outliers, such $P_{LO}$ uniformity is good enough, allowing to pump all the mixers in the array within their optimum operation regions, where less than 5% degradation of their $T_{mixer}^{DSB}$ is expected. A comparison of LO power required in our cases with other instruments in the literature is provided in [63].

These arrays have met the performance requirements demanded by the instrument and were used on board of GUSTO during its successful flight. Here we report only three arrays, however, we have also built and characterized two backup arrays (five arrays in total). One backup array was optimized for 1.6 THz and could have been used to replace either the B1 array or the B2 array, while the other one is optimized for 4.7 THz to replace the B3 array if necessary.

We now compare the mixer performance in our arrays with some of the best single pixel results reported previously in the literature, and with the performance of other instruments in the next paragraph. Our average $T_{mixer}^{DSB}$of 330K at 2GHz IF, at 1.46 THz (for B1) is very similar to a $T_{mixer}^{DSB}$ of 300 K at 1.5 GHz IF (measured at 1.3 THz) reported by K. M. Zhou et al [64,65], which was derived from their $T_{rec}^{DSB}$(600 K) and the optical losses. Our average $T_{mixer}^{DSB}$ of 420 K at 2 GHz IF obtained at 1.9 THz (B2) is close to what was reported in our labs, by Zhang et al [13], where a $T_{mixer}^{DSB}$ of 380 K at 1.5 GHz IF is derived. Additionally, our result for B2 array is also in line with or even better than the single pixel $T_{rec}^{DSB}$ of 900 K at 1.5 GHz IF, reported by Kloosterman et al [66], where we are not able to extract a $T_{mixer}^{DSB}$ due to missing details. Our average $T_{mixer}^{DSB}$ of 700 K at 2 GHz IF, at 4.7 THz (B3) is about 17% higher than the best value reported for a single pixel

in our labs, by Kloosterman et al [67], for which we estimate $a\ T_{mixer}^{DSB}$ of 600 K at 2 GHz IF. The difference can be attributed to the loss in the antenna and the use of the smaller Si lenses (5 mm) as discussed previously.

Our arrays, integrated in the GUSTO instrument, have shown a preflight performance as follows: for B1 at 1.4 THz an averaged GUSTO receiver noise temperature, $T_{rec,GUSTO}^{DSB}$, of 870 K; for B2 at 1.9 THz an averaged $T_{rec,GUSTO}^{DSB}$ of 1100 K; and for B3 at 4.7 THz an averaged $T_{rec,GUSTO}^{DSB}$ of 1920 K. All the $T_{rec,GUSTO}^{DSB}$ values above are taken at a physical temperature of 5.1 K for the mixers and an IF frequency of 1 GHz. To compare with our expected receiver noise temperatures in Table 5 the measured values should be converted using a factor of 1.11 which represents the increase in noise temperature from 1 to 2 GHz IF (16% degradation) combined with the lower temperature of the detectors in our measurements (5% improvement). Therefore, the measured $T_{rec,GUSTO}^{DSB}$ are slightly worse than what we expected in Table 5. This can be explained by the fact that in our lab setup for Y-factor measurements, before integration, the entire beam pattern is coupled to the hot/cold load, whereas in GUSTO there is sidelobe spillover throughout the optics and especially beam vignetting in some optical elements for some of the mixers. These effects contribute to the increase of the noise temperature, and hence the differences seen. The GUSTO performance in flight is out of scope of the present paper and will be addressed in an upcoming publication.

### 4.3. Scaling the pixel count in HEB mixer arrays

Although the arrays for GUSTO were designed in a 4×2 configuration, the need for both B1 and B2 arrays to be placed side by side on the cold plate of the instrument will demonstrate practically a 4×4 mixer array using our array architecture. In this case, care should be taken to ensure the pointing direction of the mixers in one array to be parallel to those from another array. The accurate pointing of 8 mixers within one array has been demonstrated [48]. Furthermore, in the case of B1 and B2 the final pointing was achieved relative to the same reference, effectively demonstrating the accurate pointing of the pixels between the two arrays.

The above approach allows to extend an array with more pixels, for example, an 8x8 pixel array. We argue that we can also build in principle eight 4x2 sub-arrays with the right mechanical adaptations, which can be assembled, characterized for their sensitivity and beam pointing independently, and then are mounted on the cold plate of an instrument, like GUSTO. In terms of the LO, for 1.46 THz, one can build eight sub-arrays of LO based on frequency multiplier chains and combine them to form 64 LO beams. At the higher frequencies, including 1.9 THz, a combination of a QCL with a phase grating could be used to generate 64 LO beams. High power QCLs have been demonstrated, for example, a 4.7 THz QCL with an output power of 8 mW at 55 K [23] and a 1.8 THz QCL with an output power of 28 mW at 10K [70]. Based on the GUSTO experience, about 10 mW will be sufficient to pump a 64 pixel array. Additionally, a phase grating to generate 81 beams from a single QCL with a high efficiency (94 %) has been demonstrated in [71], that can be applied for generating 64 beams as well. Therefore, we conclude that a large HEB array receiver of 64 pixels is feasible using current array approach and testing facilities.

To further expand the array, e.g., ≥100 pixels, one should explore an integrated approach similar to what was used for the direct detector array [72], which consists essentially of an array of lenses fabricated on a wafer and an array of HEBs also on a wafer. The mixer array is formed by aligning two wafers, that may offer a reliable and cheap technology for future large heterodyne arrays. The concept study of this new approach, including the choices of low noise amplifiers and spectrometers, has been described in detail in [73]. However, until such a solution is available, our approach can provide a feasible route for larger heterodyne HEB arrays, for example, for the proposed concept instruments HERO [33] or the far-infrared spectroscopic surveyor (FIRSS) [34].

## 5. CONCLUSIONS

We have successfully demonstrated three 4×2 heterodyne HEB arrays for GUSTO, which were operated at local oscillator frequencies of 1.46, 1.9 and 4.7 THz, respectively. These arrays consist of NbN HEB mixers, where elliptical lenses and spiral antennas are applied to couple the radiation. These arrays represent, to date, the highest pixel count using the quasi-optical scheme at supra-THz frequencies. We have experimentally characterized the arrays over three key parameters, namely the mixer noise temperature ($T_{mixer}^{DSB}$), mixer conversion loss ($L_{mixer}^{DSB}$), and optimal LO power ($P_{LO}$) at the HEB. Our results demonstrate the heterodyne arrays with not only excellent sensitivity, which for example at 4.7 THz is only 6.2 times the quantum noise (hf/2k), but also good uniformity of the performance parameters. The latter is critical for efficient operation of an array within the instrument. Additionally, the measured receiver temperatures at the three frequencies, when arrays are installed in the GUSTO instrument, are also shown. GUSTO launched from Antarctica on

the 31st December 2023 having a successful flight of 57 days, the longest ever recorded by NASA for such mission profile. Additionally, our array architecture based on quasi-optical mixers can be scaled up to a large array, e.g., 64 pixels, opening a new avenue towards large heterodyne arrays suitable for future space missions.

## APPENDIX I – CONVERSION GAIN METHODOLOGY VERIFICATION

The typical methodology for measuring the conversion loss requires the use of a circulator between HEB and LNA, as described in [54]. However, our heterodyne measurement setup was designed to measure receiver noise temperatures as well as the IF noise bandwidth, necessitating a range of 0.5-4 GHz for which no suitable circulators are available. Nonetheless, a modified version of the U factor [53] can be used to determine the conversion loss if certain conditions are met: the HEB detector can act as a microwave short, and the cryogenic low noise amplifier must exhibit very low reflection coefficients ($S_{11}$).

The first condition is satisfied when the detector is in its superconducting state, causing the HEB to reflect back all power from the LNA. The second condition is also met by our SiGe cryogenic amplifier, which has a relatively low $S_{11}$ within the IF frequencies of interest for the conversion loss measurements. In our case our LNA has a $S_{11}$ of -20 dB at 2 GHz. This allows us to assume that all the signals from the HEB, either in the operation to respond the hot load or in the superconducting state, transmit through the LNA. With these conditions validated, we can apply the U factor equation, but with $T_{REF}=T_{IF}=6.5K$, instead of the temperature of the 50 Ω resistor in a circulator, typically 4.2 K. We apply this modified U-factor technique in the present paper.

To validate this approach experimentally, we characterized an HEB mixer around 2 GHz., similar to those used in the GUSTO arrays, both with and without a circulator between the HEB mixer and the SiGe LNA. Without the circulator, we applied the modified U factor technique as described previously, while with the circulator, we used the standard U factor expression. Measurements showed an approximate 1.1 dB increase in conversion loss when using the circulator. Given the circulator's insertion loss of 0.7 dB (at room temperature), the actual difference between the two methods is approximately 0.4 dB. This small difference in conversion loss values indicates that our approach is sufficiently accurate. As the devices used in our arrays are very similar, we consider the observed difference to be the expected error margin in our conversion loss data, i.e., ±0.4 dB. This small error gives an only 1 % uncertainty of derived mixer noise temperatures in our case.

## ACKNOWLEDGEMENTS

We acknowledge the technical support from Jarno Panman, Rob van der Schuur, Erik van der Meer, Henk Ode, Duc Nguyen, Marcel Dijkstra. We also thank Yuner Gan, Axel Detrain, Geert Keizer, Gabby Aitink-Kroes, Brian Jackson and Willem Jellema for helpful discussions.

## REFERENCES

[1] C. K. Walker, “THz coherent detection systems,” in Terahertz Astronomy, 1st ed. New York, NY, USA: Taylor & Francis, 159–227 (2016).

[2] C. Pabst, R. Higgins, J. R. Goicoechea, D. Teyssier, O. Berne, E. Chambers, M. Wolfire, S. T. Suri, R. Guesten, J. Stutzki, U. U. Graf, C. Risacher, and A. G. G. M. Tielens, “Disruption of the Orion molecular core 1 by wind from the massive star θ 1 Orionis C”, Nature, **565**, 7741, 618–621 (2019) .

[3] Y. M. Seo, P. F. Goldsmith, C. Walker, D. J. Hollenbach, M. G. Wolfire, C. Kulesa, V. Tolls, P. N.Bernasconi, Ü. Kavak, F. F. S. van der Tak, R. Shipman, J. R. Gao, A. Tielens, M.G. Burton, H. York, E. Young, W. L. Peters, A. Young, C. Groppi, K. Davis, J. L. Pineda, W. D. Langer, J. H. Kawamura, A. Stark, G. Melnick, D. Rebolledo, G. F. Wong, S. Horiuchi and T. B. Kuiper, “Probing ISM Structure in Trumpler 14 and Carina I Using the Stratospheric Terahertz Observatory 2”, Astrophys. J., **878**, 2 (2019).

[4] K. Tadaki, D. Iono, M. S. Yun, I. Aretxaga, B. Hatsukade, D. H. Hughes, S. Ikarashi, T. Izumi, R. Kawabe, K. Kohno, M. Lee, Y. Matsuda, K. Nakanishi, T. Saito, Y. Tamura, J. Ueda, H. Umehata, G. W. Wilson, T. Michiyama, M. Ando and P. Kamieneski, “The gravitationally unstable gas disk of a starburst galaxy 12 billion years ago”, Nature **560**, 613-616 (2018).

[5] R. Güsten, H. Wiesemeyer, D. Neufeld, K. M. Menten, U. U. Graf, K. Jacobs, B. Klein, O. Ricken, C. Risacher and J. Stutzki, “Astrophysical detection of the helium hydride ion HeH+”, Nature **56**, 357-359 (2019).

[6] H. Linz, H. Beuther, M. Gerin, J. Goicoechea, F. Hemich, O. Krause, Y. Liu, S. Molinari, V. Ossenkopf-Okada, J. Pineda, M. Sauvage, Eva Schinnerer, F. van der Tak, M. Wiedner, J. Amiaux, D. Bhatia, L. Buinhas, G. Durand, R. Forstner ,U. Graf, M. Lezius, "Bringing high spatial resolution to the far-infrared", Exp. Astronomy **51**, 661-697 (2021).
[7] P. L. Richards, T. M. Shen, R. E. Harris, and F. L. Lloyd, "Quasiparticle heterodyne mixing in SIS tunnel junctions", Applied Physics Letters, **34**, 5, 345–347 (1979).
[8] J. R. Tucker and M. J. Feldman, "Quantum detection at millimeter wavelengths", Rev. Modern Phys., **57**, 1055–1113 (1985).
[9] E E. Gershenzon, G. Gol'tsman, I. Gogidze, Y. Gousev, A. Elant'ev, B. Karasik, and A. Semenov, "Millimeter and submillimeter range mixer based on electron heating of super conducting films in the resistive state", Superconductivity, **3**, 10, 1582–1597, (1990).
[10] T. M. Klapwijk and A. V. Semenov, "Engineering physics of superconducting hot-electron bolometer mixers", IEEE Trans. Terahertz Sci. Technol. **7**, 627–648, (2017).
[11] D. Farrah, K. Ennico, D. Ardila, et al, "Review: far-infrared instrumentation and technological development for the next decade", Journal of Astron. Telescopes, Inst. And systems, **5**, 2, 020901 (2019).
[12] A. Wootten and A. R. Thompson, "The Atacama Large Millimeter/Submillimeter Array", Proc. IEEE, **97,** 8, 1463–1471 (2009).
[13] W. Zhang, P. Khosropanah, J. R. Gao, E. L. Kollberg, K. S. Yngvesson, T. Bansal, R. Barends and T. M. Klapwijk, "Quantum noise in a terahertz hot electron bolometer mixer", Appl. Phys. Lett. **96**, 111113, (2010).
[14] M. Hajenius, J.J.A. Baselmans, A. Baryshev, J.R. Gao, T.M. Klapwijk, J.W. Kooi, W. Jellema, and Z.Q. Yang, "Full characterization and analysis of a terahertz heterodyne receiver based on a NbN hot electron bolometer", J. Appl. Phys., **100**, 074507 (2006).
[15] S. Cherednichenko, V. Drakinskiy, T. Berg, P. Khosropanah and E. Kollberg, "Hot-electron bolometer terahertz mixers for the Herschel Space Observatory", Review of Sci. Instruments, **79**, 034501 (2008).
[16] T. de Graauw et al., "The Herschel-Heterodyne Instrument for the Far-Infrared (HIFI)", Astron. Astrophys., **518**, no. L6, 1–7 (2010).
[17] C. Walker, C. Kulesa, P. Bernasconi, H. Eaton, N. Rolander, C. Groppi, J. Kloosterman, T. Cottam, D. Lesser, C. Martin, A. Stark, D. Neufeld, C. Lisse, D. Hollenbach, J. Kawamura, P. Goldsmith, W. Langer, H. Yorke, J. Sterne, A. Skalare, I. Medhi, S. Weinreb, J. Kooi, J. Stutzski, U. Graf, M. Brasse, C. Honingh, R. Simon, M. Akyilmaz, P. Puetz and Mark Wolfire, "The Stratospheric THz Observatory (STO)", Proc. SPIE, Millimeter, Submillimeter, and Far-Infrared Detectors and Instrumentation of Astronomy VII, Austin, TX, USA, **7733**, 77330N-1 (2010).
[18] C. Risacher, R. Güsten, J. Stutzki, H.-W. Hübers, R. Aladro, A. Bell, C. Buchbender, D. Büchel, T. Csengeri, C. Duran, U. U. Graf, R. D. Higgins, C. E. Honingh, K. Jacobs, M. Justen, B. Klein, M. Mertens, Y. Okada, A. Parikka, P. Pütz, N. Reyes, H. Richter, O. Ricken, D. Riquelme, N. Rothbart, N. Schneider, R. Simon, M. Wienold, H. Wiesemeyer, M. Ziebart, P. Fusco, S. Rosner and B. Wohler, "The upGREAT Dual Frequency Heterodyne Arrays for SOFIA", Journal of Astronomical Instrumentation, **7**, 4, 1840014 (2018).
[19] J. V. Siles, R. H. Lin, C. Lee, E. Schlecht, A. Maestrini, P. Bruneau, A. Peralta, J. Kloosterman, J. Kawamura and I. Mehdi, "Development of High-Power Multi-Pixel LO Sources at 1.47 THz and 1.9 THz for Astrophysics: Present and Future", Proc. 26th International Symposium on Space Terahertz Technology T1-3, 40 (2015).
[20] I. Mehdi, J. V. Siles, C. Lee and E. Schlecht, "THz Diode Technology: Status, Prospects, and Applications", Proc. IEEE. **105**, 6, 990-1007 (2017).
[21] B. S. Williams, "Terahertz quantum-cascade lasers", Nat. Photonics **1**, 517–525 (2007).
[22] M. S. Vitiello, G. Scalari, B. Williams, and P. De Natale, "Quantum cascade lasers: 20 years of challenges", Optics Express, **23**, 4, 5167–5182 (2015).
[23] A. Khalatpour, A. K. Paulsen, S. J. Addamane, C. Deimert, J. L. Reno, Z. R. Wasilewski and Q. Hu, "A tunable Unidirectional Source for GUSTO's Local Oscillator at 4.74 THz", IEEE Trans. Terahertz Sci. Technol., **12**, 2, 144-150 (2021).
[24] C. A. Curwen, J. L. Reno and B. S. Williams, "Broadband continuous single-mode tuning of a short-cavity quantum-cascade VESCEL", Nat. Photonics **13**, 855-859 (2019).
[25] B. Mirzaei, J. R. G. Silva, W. J. Vreeling, W. Laauwen, D. Ren and J. R. Gao, "Enhanced Sensitivity of THz NbN Hot Electron Bolometer Mixers", submitted to IEEE Transactions on Terahertz Science and Technology (or https://doi.org/10.48550/arXiv.2311.02613)
[26] J. A. Murphy, R. Padman and R. E. Hills, "An experimental submillimeter heterodyne array receiver", International Journal of Infrared and Millimeter Waves, **9**, 4, 325–350 (1988).
[27] U. U. Graf, C. E. Honingh, K. Jacobs, J. Stutzki, "Terahertz Heterodyne Array Receivers for Astronomy", J. Infrared Milli. Terahertz waves, **36**, 896-921 (2015).
[28] P. F. Goldsmith, "Sub-millimeter heterodyne focal-plane arrays for high-resolution astronomical spectroscopy", URSI Radio Sci. Bull. **362**, 53-73 (2017).
[29] C. Walker, C. Kulesa, A. Young, W. Verts, J. R. Gao, Q. Hu, J. Silva, B. Mirzaei, W. Laauwen, J. Hesler, C. Groppi, and A. Emrich, Gal/Xgal U/LDB Spectroscopic/ Stratospheric THz Observatory: GUSTO, Proc. SPIE, **12190**, 121900E (2022).
[30] J. R. G. Silva, B. Mirzaei, W. Laauwen, N. More, A. Young, C. Kulesa, C. Walker, A. Khalatpour, Q. Hu, C. Groppi and J. R. Gao, "4×2 HEB receiver at 4.7 THz for GUSTO", Proc. SPIE **10708**, 107080Z (2018).
[31] J. Siles, J. Pineda, J. H. Kawamura, C. Groppi, P. Bernasconi, J. Gundersen, P.F. Goldsmith, "ASTHROS - Astrophysics Stratospheric Telescope for High-Spectral Resolution Observations at Submillimeter-waves: Mission Overview and Development Status", Proceedings 31st ISSTT, 5 (2020).

[32] C. K. Walker, G. Chin, S. Aalto, C. M. Anderson, J. W. Arenberg, C. Battersby, E. Bergin, J. Bergner, N. Biver, G. L. Bjoraker, J. Carr, T. Cavalié, E. De Beck, M. A. DiSanti, P. Hartogh, L. K. Hunt, D. Kim, Y. Takashima, C. Kulesa, D. Leisawitz, J. Najita, D. Rigopoulou, K. Schwarz, Y. Shirly, A. A. Stark, X. Tielens, S.Viti, D. Wilner, E. Wollack, E. Young, "Orbiting Astronomical Satellite for Investigating Stellar Systems (OASIS) : following the water trail from the interstellar medium to oceans", Proc. SPIE, **11820**, 1182000 (2021).
[33] M. C. Wiedner, I. Mehdi, A. Baryshev, V. Belitsky, V. Desmaris, A. DiGiorgio, et al., "A Proposed Heterodyne Receiver for the Origins Space Telescope", IEEE Trans. Terahertz Sci. Technol. **8**, 6, 558-571 (2018).
[34] D. Rigopoulou, C. Pearson, B. Ellison, M. Wiedner, V. O. Okada, B. K. Tan, I. Garcia-Bernete, M. Gerin, G. Yassin, E. Caux, S. Molinari, J. R. Goicoechea, G. Savini, L. K. Hunt, D. C. Lis, P. F. Goldsmith, S. Aalto, G. Magdis and C. Kramer, "The far-infrared spectroscopic surveyor (FIRSS)", Exp. Astronomy **51**, 699 (2021).
[35] J. Hesler, S. Retzloff, C. Gardner, S. Mancone, B. Swartz, C. Rowland, and T. Crow, "Development and Testing of the 1.46 THz and 1.9 THz GUSTO Flight-Model Local Oscillator Arrays", Proc. 31st ISSTT, 36 (2020).
[36] A. Khalatpour, J. L. Reno, and Q. Hu, "Phase-locked photonic wire lasers by π coupling", Nat. Photonics, 13, 47-53 (2019).
[37] H. Richter, M. Wienold, L. Schrottke, K. Biermaan, H. Grahn and H. Hubers, "4.7-THz Local Oscillator for the GREAT Heterodyne Spectrometer on SOFIA", IEEE Trans. Terahertz Sci. and Techn., **5**, 4, 539-545 (2015).
[38] B. Mirzaei, Y. Gan, M. Finkel, C. Groppi, A. Young, C. Walker, Q. Hu, and J. R. Gao, "4.7 THz asymmetric beam multiplexer for GUSTO", Opt. Express **29**, 15, 24434-24445 (2021).
[39] J. V. Siles, R. Lin, P., Lee, C. Bruneau, and I. Mehdi, "An ultra-compact 16-pixel local oscillator at 1.9 THz.", Proc. 41st International Conference on Infrared, Millimeter, and Terahertz Waves (2016).
[40] A. Gatesman, R. Giles and J. Waldman, "High-precision reflectometer for submillimeter wavelengths", J. Opt. Soc. Am. B, **12**, 2, 212-219 (1995).
[41] W. Zhang, P. Khosropanah, J. R. Gao, T. Bansal, T. M. Klapwijk, W. Miao and S. C. Shi, "Noise temperature and beam pattern of an NbN hot electron bolometer mixer at 5.25 THz", J. Appl. Phys 108, 093102 (2010).
[42] A. D. Semenov, H. Richter, H. Hubers, B. Gunther, A. Smirnov, K. S. Il'in, M. Siegel and J. P. Karamarkovic, "Terahertz Performance of Integrated Lens Antennas With a Hot-Electron Bolometer", IEEE Transactions on Microwave Theory and Techniques, **55**, 2, 239-247 (2007).
[43] W. Zhang, J. R. Gao, M. Hajenius, W. Miao, P. Khosropanah, T. M. Klapwijk, and S. C. Shi, "Twin-Slot Antenna Coupled NbN Hot Electron Bolometer Mixer at 2.5 THz", IEEE Transactions on Terahertz Science and Technology, **1**, 2, 378 -382 (2011).
[44] The logarithmic spiral antenna used has a starting radius k=4μm, curvature a=0.318 and arm width δ=83 deg.
[45] B. D. Jackson, "NbTiN-Based THz SIS Mixers for the Herschel Space. Observatory", PhD dissertation, Fac. of App. Sci., TU Delft, NL (2005).
[46] J. R. G. Silva, M. Finkel, W. M. Laauwen, S. J. C. Yates, B. Mirzaei, N. Vercruyssen, A. Young, C. Kulesa, C. Walker, F. van der Tak and J. R. Gao, " Beam waist properties of spiral antenna coupled HEB mixers at Supra-THz frequencies", IEEE Transactions on Terahertz Sci. and Tech., **13**, 2, 167 – 177 (2023).
[47] A. Gatesman, J. Waldman, M. Ji, C. Musante and S. Yngvesson, "An anti-reflection coating for silicon optics at terahertz frequencies", IEEE Microwave and guided wave letters, **10**, 7, 264-266 (2000).
[48] J. R. G. Silva, M. Finkel, W. M. Laauwen, M. Westerweld, N. More, A. Young, C. Kulesa, C. Walker, F. van der Tak and J. R. Gao, "High Accuracy Pointing for Quasi-optical THz Mixer Arrays", IEEE Trans. Terahertz Sci. Technol. **12**, 1, 53-62 (2022).
[49] D. J. Hayton, J. R. Gao, J. W. Kooi, Y. Ren, W. Zhang and G. De Lange, "Stabilized hot electron bolometer heterodyne receiver at 2.5 THz", Appl. Phys. Letter, **100**, 8, 081102 (2012).
[50] S. Weinreb, J. Bardin, H. Mani and G. Jones, "Matched wideband low-noise amplifiers for radio astronomy", Review of Scientific Instruments **80**, 044702 (2009).
[51] P. Khosropanah, J. R. Gao, W. M. Laauwen and M. Hajenius, "Low noise NbN hot electron bolometer mixer at 4.3THz", Appl. Phys. Lett. **91**, 221111 (2007).
[52] M. Hajenius, J. J. A. Baselmans, A. Baryshev, J. R. Gao, T. M. Klapwijk, J. W. Kooi, W. Jellema, and Z. Q. Yang, "Full characterization and analysis of a terahertz heterodyne receiver based on a NbN hot electron bolometer," J. Appl. Phys., **100**, 074507-1–074507-10, Oct. (2006).
[53] E. Novoselov, S. Bevilacqua, S. Cherednichenko, H. Shibata and Y. Tokura, "Effect of the Critical and Operational Temperatures on the Sensitivity of MgB HEB Mixers", IEEE Transactions on Terahertz Science and Technology, **6**, 2, 238-244 (2016).
[54] S. Cherednichenko, M. Kroug, H. Merkel, P. Khosropanah, A. Adam, E. Kollberg, D. Loudkov, G. Gol'tsman, B. Voronov, H. Richter, and H. Huebers, "1.6 THz heterodyne receiver for the far infrared space telescope", Phys. C: Supercond. and Its Applicat. **427**, 372 (2002).
[55] H. Ekström, B. S. Karasik, E. Koll erg and K. S. Yngvesson, "Conversion gain and noise of niobium superconducting hot-electron-mixers", IEEE Trans Microw. Theory Tech. **43**, 4, 938-947 (1995).
[56] To characterize the mixer at 4.7 THz we used a QCL with a frequency of 4.68 THz as LO. Because of the high absorption in air at this frequency we performed both measurements at 5.25 and 4.68 THz using a vacuum setup, being similar to the one reported in [65]. In our case there is a rotating mirror with 32 mm diameter at 170mm from the HEB, with the cold load being 35 mm in diameter 60 mm after the mirror.
[57] J. R. Gao, M. Hajenius, F. D. Tichelaar, T. M. Klapwijk, B. Voronov, E. Grishin, G. Gol'tsman, C. A. Zorman and M. Mehregany, "Monocrystalline NbN nanofilms on a 3$\mathcal{C}$-SiC/Si substrate", Applied Physics Letters **91**, 062504 (2007).

[58] J. W. Kooi, J. J. A. Baselmans, M. Hajenius, J. R. Gao, T. M. Klapwijk, P. Dieleman, A. Baryshev, and G. de Lange, "IF impedance and mixer gain of NbN hot electron bolometers", J. Appl. Phys. **101**, 4, 044511(2007).
[59] D. J. Hayton, J. L. Kloosterman, Y. Ren, T.Y. Kao, J. R. Gao, T. M. Klapwijk, Q. Hu, C. K. Walker and J. L. Reno, "A 4.7THz heterodyne receiver for a balloon borne telescope", Proc. SPIE **9153**, 91531R (2014).
[60] W. Zhang, W. Miao, J. Q. Zhong, S. C. Shi, D. J. Hayton, N. Vercruyssen, J. R. Gao and G. N. Goltsman, "Temperature dependence of the receiver noise temperature and IF bandwidth of superconducting hot electron bolometer mixers", Supercond. Sci. Technol. **27**, 085013 (2014).
[61] J. R. G. Silva, R. Farinha, D. J. Hayton, W. Laauwen, B. Mirzaei, N. More, A. Young, C. Kulesa, C. Walker and J. R. Gao, "Preliminary design study of a 4× 2 HEB array at 4.7 THz for GUSTO", Proc. 29th ISSTT, 82-86 (2018).
[62] E. L. Kollberg, K. S. Yngvesson, Y. Ren, W. Zhang, P. Khosropanah, and J. R. Gao, "Impedance of Hot-Electron Bolometer Mixers at Terahertz Frequencies", IEEE Trans. Terahertz Sci. Technol. **1**, 2, 383-389 (2011).
[63] The LO power required at the HEB for the GUSTO arrays is very similar to those used for other instruments. For example, the HIFI HEBs required 200-500 nW [15]; the HEBs at 1.4 THz in STO-2 required ~220nW, whereas those at 1.9 THz required a bit lower ~ 110 nW [66]. The devices in upGREAT require ~300 nW [67].
[64] K. M. Zhou, W. Miao, Z. Lou, J. Hu, S. L. Li, W. Zhang, S. C. Shi, R. Lefevre, Y. Delorme, and T. Vacelet, "1.4 THz Quasi-optical NbN Superconducting HEB Mixer Developed for the DATE5 Telescope", IEEE transactions on Applied superconductivity, **25.** 3, 1-5 (2014).
[65] R. Lefèvre, Y. Jin, A. Féret, T. Vacelet, W. Miao, L. Pelay, F. Dauplay, M. Ba-Trung, G. Gay, J.-C. Villégier, J. Spatazza, J.-M. Krieg, and Y. Delormeet al, "Terahertz NbN hot electron bolometer fabrication process with a reduced number of steps", Proc. of the 23rd ISSTT, 127 (2012).
[66] J. L. Kloosterman, J. H. Kawamura, A. J. Tang, R. Kim, J. Siles, F. Boussaha, B. Bumble, C. Lee, A. Peralta, R. Lin, I. Medhi, "4-Pixel Heterodyne Receiver at 1.9 THz using a CMOS Spectrometer", Proc. of the 28th ISSTT, 74, 2017.
[67] J. L. Kloosterman, D. J Hayton, Y. Ren, T. Kao, J.N. Hovenier, J. R. Gao, T. M. Klapwijk, Q. Hu, C. K Walker and J. L. Reno, "Hot electron bolometer heterodyne receiver with a 4.7-THz quantum cascade laser as a local oscillator", Appl. Phys. Lett. **102**, 011123 (2013).
[68] A. Young, C. Walker, C. Kulesa, P. Bernasconi, R. Dominguez, J. Siles, D. Hayton, J. R. Gao, W. Peters, P. Goldsmith, "Stratospheric Terahertz Observatory 2016, Sub-orbital flight from McMurdo, Antarctica", Proceedings ISSTT, 4 (2017).
[69] D. Büchel, P. Pütz, K. Jacobs, M. Schultz, U. U. Graf, C. Risacher, H. Richter, O. Ricken, H. Hübers, R. Güsten, C. E. Honingh, and J. Stutzki, "4.7-THz Superconducting Hot Electron Bolometer Waveguide Mixer", IEEE Trans. Terahertz Sci. Technol. **5**, 2, 207-214 (2015).
[70] S. Kumar, C. Chan, Q. Hu, and J. L. Reno, "A 1.8-THz quantum cascade laser operating significantly above the temperature of $\hbar\omega$/kB", Nature Phys. **7**, 166–171 (2011).
[71] Y. Gan, B. Mirzaei, J. R. G. Silva, A. Khalatpour, Q. Hu, C. Groppi, J. V. Siles, F. van der Tak, and J. R. Gao, "81 supra-THz beams generated by a Fourier grating and a quantum cascade laser", Opt. Express **27**, 34192-34203 (2019).
[72] J. Bueno, V. Murugesan, K. Karatsu, D. Thoen and J. J. Baselmans, "Ultrasensitive Kilo-Pixel Imaging Array of Photon Noise-Limited Kinetic Inductance Detectors Over an Octave of Bandwidth for THz Astronomy", J. of Low Temperature Physics, **193**, 96-102 (2018).
[73] Y. Gan, Chapter 8, "Development of large terahertz heterodyne receiver arrays for future space observations", PhD dissertation, University of Groningen (2021).